Particle Accelerators, Vol. 63, pp. 79–103
Reprints available directly from the publisher
Photocopying permitted by license only

FREQUENCY MAP ANALYSIS OF AN INTENSE MISMATCHED BEAM IN A FODO CHANNEL

A. BAZZANI[a,*], M. COMUNIAN[b] and A. PISENT[b]

[a]*INFN Sezione di Bologna and University of Bologna, Via Irnerio, 46, I-40126, Bologna, Italy;* [b]*INFN Laboratori Nazionali di Legnaro, Via Romea 4, I-35020, Padova, Italy*

(Received 14 July 1998; In final form 18 November 1998)

The comprehension of the mechanism that leads to small beam losses is one of the key points for the feasibility of the next generation of high power linacs. In this paper we study the nonlinear dynamics of the beam halo particles in a FODO channel, by using the Frequency Map analysis. This tool provides a picture which allows to detect the regular, resonant or chaotic regions also in the phase space for a mismatched beam in two degrees of freedom. Moreover we introduce a criterion for single particle stability and we make comparisons with tracking results.

Keywords: Beam dynamics; Linac; Frequency map; Beam halo

1 INTRODUCTION

Proton linacs with beam intensities between 10 and 120 mA, for a beam power up to 100 MW, are under study in various laboratories, for applications that go from fundamental physics to energy production and nuclear waste transmutation.[1] These performances will represent a big step forward with respect to the present linac technology, and one of the most critical aspects is the control of beam losses. Typically, losses lower than 1 W/m are needed to allow hands on maintenance in case of fault.[2] Moreover a significant reduction of beam

* Corresponding author. E-mail: bazzani@bo.infn.it.

losses simplifies the problem of the stocking of activated parts and causes a smaller environmental impact.

These losses are associated with the presence of a beam halo, populated by very few particles but with a radius significantly larger than the beam root mean square (rms) radius up to the bore hole. A great theoretical effort is presently devoted to the understanding of halo formation.[3–6]

A realistic simulation of an intense beam in a linac, able to follow 10^8–10^9 particles in a self-consistent way, taking into account the various scattering processes, the interaction with the vacuum pipe, and whatever happens in a real linac, is a too formidable task even for modern computers. Some simplifications are generally introduced, in order to determine more handy systems that include anyway the most relevant physical aspects. Many theoretical and experimental studies have concentrated on the two degrees of freedom problem determined by a collisionless continuous beam propagating in a FODO focusing channel. This problem involves many features of the three degrees of freedom system which describes the propagation of a bunched beam in a linear accelerator.

The space charge forces, acting on single particles, mainly determine this behavior, due to the nonlinear forces. The problem can be simplified considerably considering the space charge forces as generated by the core of the beam (particle–core model), and calculating the core evolution using the method of the equivalent KV (Kapchinsky Vladimirsky) beam.[7] Leaving the self-consistency, the single particle problem can be treated using the dynamical systems tools. In particular, particles immediately outside the core can reach big amplitudes and form the halo due to nonlinear resonances and chaoticity in the phase space. The mechanism for the spill of a few particles from the core to the halo could be, for example a small nonlinearity of the space charge force inside the beam (deviation from KV distribution,[5] image charges on the pipe...) or a low probability scattering process.

In this paper we have studied the beam dynamics in a FODO channel using the particle–core model. We have faced a specific problem: many simulations show that the halo formation is enhanced by the mismatching of the beam core. In this case the Hamiltonian system associated to the betatronic motion of the test particle is not periodically dependent on the longitudinal coordinate due to the

non-periodicity of the envelope of the beam. The direct plot of the phase space obtained by using a Poincarè section does not allow to distinguish regular orbit from chaotic ones. In this paper we use the method of the frequency map analysis to represent the phase space.[8–10] This method has been applied to celestial mechanics[8] and accelerator physics,[11–14] to study the stability of the orbits, and turns out to be very efficient to detect the location of resonances and the chaotic regions. Moreover it is not affected by the non-periodicity of the Hamiltonian systems and can be extended to two or three degrees of freedom systems.

To apply the frequency map analysis in a linear magnetic lattice we assume that the FODO cells repeat identically, whereas small differences are unavoidable in the real machines. These differences could be treated as random perturbations of an average dynamics and the informations provided by the frequency map (FM) are useful for a statistical analysis.

In Section 2 we describe the particle–core model, we introduce the equation of motion for a test particle, the periodic beam envelope and the envelope breathing modes.

In Section 3 we describe the focusing channel used for this study.

In Section 4 we describe the method of the frequency map analysis and we discuss its application to our case.

In Section 6 we show the numerical results of our FM analysis of the two degrees of freedom system, describing a beam propagating in a FODO cell. We compare the FM results with tracking, and therefore, choosing the initial points on the basis of the FM, we show a systematic study of the maximum particle amplitude as a function of envelope mismatch.

2 THE PARTICLE–CORE MODEL

An intense proton beam propagating in an accelerating structure can generally be treated as a Poisson–Vlasov problem. The particle distribution generates a field (self-field) that can be computed by solving the Poisson equation in the beam frame, and the distribution evolves according to a Vlasov equation, in which the superposition of external fields and self-fields is introduced. A solution of such a system is

called self-consistent beam evolution. This approach is approximated, since collisions and effects of the complete electromagnetic system are neglected, but it is generally adequate for proton linacs.

However, when we look at very small beam losses, it is reasonable to assume that these losses are associated with the irregular behavior of a few particles in the field generated by the regular particles, which form the "core" of the beam. This distinction between core and test particles is clearly a short cut, and gives solutions that are rigorously not self-consistent, but are practically correct if irregular particles are a few.

This approach gives a single particle system and the possibility of an accurate analysis of the nonlinear behaviour of the particles, using all the tools offered by the Hamiltonian mechanics. This method assumes that there exists a self-consistent periodic distribution for the beam propagating in a periodic focusing channel, like the KV distribution. For this distribution the charge density inside the beam is uniform and the single particle equations are:

$$x_j'' + K_j(s)x_j - \frac{\xi}{(\hat{a}_1 + \hat{a}_2)\hat{a}_j} x_j = 0, \qquad j = 1, 2 \tag{1}$$

where s is the longitudinal coordinate, $'$ indicates the derivative respect to s and x_j are the single particle transverse coordinates, with x_1 horizontal and x_2 vertical displacement with respect to beam axis; $\xi = [e/(\pi\epsilon_0)][I/(mc^3\beta^3\gamma^3)] = I/(I_c\beta^3\gamma^3)$ is the space charge parameter, with I beam current (peak current for a bunched beam), $I_c = 7.8 \times 10^6$ A proton characteristic current, β and γ relativistic factors; $K_j(s)$ is the external focusing, and for a pure quadrupole channel $K_1(s) = -K_2(s) = K(s)$. Moreover we define

$$\hat{a}_j = \sqrt{a_j^2 + \chi} \tag{2}$$

with $a_j = 2\sqrt{\langle x_j^2 \rangle}$ semiaxis of the elliptical beam cross section, where $\chi = 0$ if

$$\frac{x_1^2}{a_1^2} + \frac{x_2^2}{a_2^2} < 1$$

(i.e. the test particle is inside the beam core) or χ positive solution of:

$$\frac{x_1^2}{a_1^2+\chi}+\frac{x_2^2}{a_2^2+\chi}=1 \tag{3}$$

otherwise. It should be noted that for large amplitudes the beam ellipticity can be neglected ($a_1 \simeq a_2$); therefore from Eq. (3) $\hat{a}_1 = \hat{a}_2 = \sqrt{x_1^2 + x_2^2}$. As a result the space charge force in Eq. (1) reduces to the well-known $\xi x_j/[2(x_1^2 + x_2^2)]$.

The forces inside the beam are linear, and the equations of the envelope can be found with the substitution in (1) of the Floquet functions $x_j = a_j(s)\exp(i\psi_j(s))$ with

$$\psi_j' = \frac{\epsilon_j}{a_j^2}, \tag{4}$$

where the constants ϵ_j are the emittances. The resulting envelope equations are:

$$a_j'' + K_j(s)a_j - \frac{\xi}{a_1+a_2} - \frac{{\epsilon_j}^2}{a_j^3} = 0. \tag{5}$$

These equations, together with the single particle equations (1), give a coherent description of the dynamics and a self-consistent solution of the Poisson–Vlasov problem.

Equations (5) can be applied to more general cases than the KV distribution; indeed they are valid for any distribution if interpreted statistically, with $\sqrt{\langle x_j^2\rangle} = a_j/2$ and $\epsilon_j^2 = 16(\langle x_j^2\rangle\langle p_j^2\rangle - \langle x_j p_j\rangle^2)$. However for distributions different from a KV they are not a closed set of equations, since the space charge forces are not linear and the rms emittances are not constant, but determined by independent equations involving higher order momenta. Nevertheless for many distributions of practical interest the emittance can be considered constant or as an adiabatic invariant, and the envelope equations (5) can be used as a good approximation of the rms behavior of the beam.[15,16] We shall adopt this point of view.

In a focusing channel with period L one is interested in taking the initial beam conditions in order to follow the periodic (matched)

solution of the envelope equation $a_j(s+L)=a_j(s)$, since this allows the regular transport of the beam for an infinite (in principle) number of periods. The phase advance per period can be calculated from Eq. (4) according to:

$$2\pi\nu_j = \psi_j(s+L) - \psi_j(s) = \int_s^{s+L} \frac{\epsilon_j ds}{a_j^2}; \tag{6}$$

the ratio ν_j/ν_{0j}, with ν_{0j} phase advance corresponding to $\xi=0$, called tune depression, gives a measure of the importance of the space charge in a specific case.

If $\vec{a}(s)$ is periodic the single particle equations (1) are periodic and the Poincarè sections can be used for the analysis of the orbits. But in a real machine the beam will be matched to the channel with an error, and the envelope will be $a_j(s)+\delta_j(s)$, with $\vec{\delta}(s+L)\neq\vec{\delta}(s)$. In this case the equations of motion are not periodic and the Poincarè method is not well-grounded. In the next section we shall discuss a possible solution to this problem.

If the deviation from periodicity is small, it can be calculated from the linearized equations, giving rise to envelope modes that enter single particle dynamics. In particular if the focusing is smooth ($\nu_j \ll \frac{1}{4}$, $j=1,2$), one can directly calculate the equilibrium envelopes

$$a_j = \sqrt{\frac{\epsilon_j L}{2\pi\nu_j}}, \tag{7}$$

and the zero space charge tunes:

$$\nu_{0j} = \sqrt{\nu_j^2 + \frac{\xi}{4\pi^2}\frac{L^2}{(a_1+a_2)a_j}}. \tag{8}$$

The envelope modes are solution of the system

$$\delta_j'' + H_j\delta_j + h(\delta_1+\delta_2) = 0. \tag{9}$$

with $H_j = \nu_{0j}^2 + 3\nu_j^2$ and

$$h = \frac{\xi}{4\pi^2}\frac{L^2}{(a_1+a_2)^2} \tag{10}$$

The mode eigen-frequencies are:

$$\alpha_{\pm} = \sqrt{\frac{H_1 + H_2}{2} + h \pm \sqrt{\left(\frac{H_1 - H_2}{2}\right)^2 + h^2}} \tag{11}$$

and the corresponding eigenvectors are

$$\vec{\delta}_- = (-\sin\phi, \cos\phi), \qquad \vec{\delta}_+ = (\cos\phi, \sin\phi), \tag{12}$$

with

$$\phi = \frac{1}{2}\arctan\frac{2h}{H_1 - H_2} \tag{13}$$

mode mixing angle. In particular, if the focusing strength is equal in the two directions, the mixing angle is $\pi/4$ (taking the limit of Eq. (13) for positive $H_1 - H_2$) and the two modes, called respectively odd and even envelope modes,[17] have frequencies $\alpha_- = \sqrt{\nu_0^2 + 3\nu^2}$ and $\alpha_+ = \sqrt{2(\nu_0^2 + \nu^2)}$. On the contrary if the difference in focusing strength is large the mixing angle tends to zero. The lattices of practical interest are smooth enough so that the two modes calculated in smooth approximation can be recognized.

3 ANALYSIS OF A FODO

Our reference focusing is the FODO shown in Figure 1; the geometrical lengths and the emittances $\epsilon_x = \epsilon_y = 10^{-6}$ m are kept constant. In the following we vary ξ, K_F and K_D, corresponding to the two cases listed in Table I. The consequent frequencies are in Table II, where ν_0 are calculated with the usual matrix composition, and the other frequencies in smooth approximation. The envelope mode mixing angle is calculated according to (13).

These values are in the range considered for high intensity linacs; for example if we consider a proton beam at 100 MeV, the case #1 corresponds to a normalized emittance of 0.5 mm mrad, a gradient of 18 T/m and a beam peak current of 0.8 A (22 mA of beam current with a bunch length of 10°). Strictly speaking a tune depression of 80%

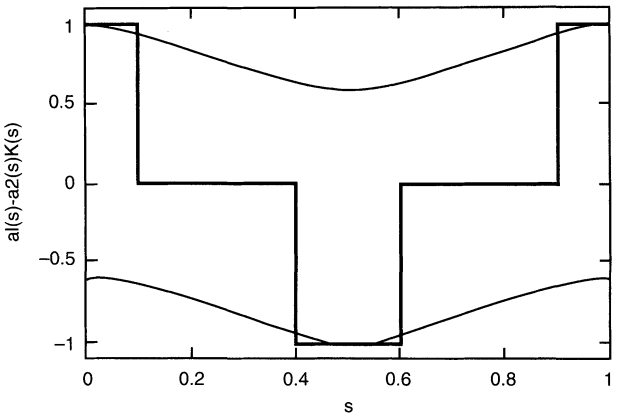

FIGURE 1 Geometry of the nominal FODO cell 1 m long; the focusing function $K(s) = K_1(s) = -K_2(s)$ is plotted, together with the matched envelopes a_1 and $-a_2$ in arbitrary units.

TABLE I Nominal cases

Case	ξ	K_F (m^{-2})	K_D [m^{-2}]
1	10^{-6}	12	12
2	10^{-6}	12.2	11.8

TABLE II Frequencies and mode mixing angles

Case	ν_{01}	ν_{02}	ν_1	ν_2	α_-	α_+	$4\phi/\pi$
1	0.168	0.168	0.136	0.136	0.29	0.31	1.0
2	0.179	0.165	0.145	0.129	0.28	0.32	0.34

does not correspond to a space charge dominated beam, but it is in the range of tune shift values interesting for the particle in core analysis; indeed in such a case the rms emittance of the beam, calculated with a multiparticle code, is not affected by the space charge and the emittance growth is negligible.

The tracking, which has been used for numerical simulations, is a kick code, which integrates both the envelope equation (5) and the single particle equation (1). Each element (quadrupole or drift space) is divided into 10 segments and the nonlinear force due to space charge is computed by means of a kick map which uses the envelope

amplitude at the center of each segment. The linear motion is computed exactly.

We have checked the precision of our tracking by comparing it with a Runge–Kutta of order four. We have computed the initial conditions for the periodic envelope with the bisection method, using the smooth approximation as an initial guess.

4 FREQUENCY MAP ANALYSIS

The analysis of the phase space by using the FM has been introduced by Laskar[8,9] to study the Hamiltonian systems in celestial mechanics. More recently the FM has been used to study the betatronic motion in hadron circular accelerators.[11–14] The theoretical foundation of the FM goes back to the KAM theory[18,19] which states the existence of a regular mapping between the set of invariant tori of a symplectic map $\mathcal{M}$ and the frequencies space. More precisely the KAM theory proves the existence of a transformation T from the action angle variables $(\vec{\theta}, \vec{I})$ to the initial variables such that the iteration of the map $\mathcal{M}$ corresponds to a shift in the angle variables

$$\mathcal{M} \circ T(\vec{\theta}, \vec{I}) = T(\vec{\theta} + \vec{\nu}(\vec{I}), \vec{I}) \tag{14}$$

where $\vec{\nu}$ are the frequencies associated to the invariant torus of the map $\mathcal{M}$ and have to satisfy some technical conditions (i.e. not too close to resonant values). As a consequence the set of invariant tori is the complement of a dense set that contains the resonant or chaotic orbits. When the perturbation is small the measure of irregular orbits is small too. We define the FM as the map which associates to each invariant torus the frequencies $\vec{\nu}$ according to Eq. (14). If the map $\mathcal{M}$ is linear, all the invariant tori have the same frequencies and the FM reduces to a single point.

If we choose a transverse section of the phase space (i.e. a section which intersects all the invariant tori in a single point) the FM turns out to be a map from the points of the section and the space of frequencies. There is no general procedure to find a transverse section for a generic Hamiltonian system, but in the case of a perturbed system, the transverse section of the unperturbed Hamiltonian is usually a

good choice for the complete system. Then we consider a uniform grid of points in the transverse section; in a region mostly filled by invariant tori, the image of the grid points in the frequencies space given by the FM is a smooth deformation of the initial grid since almost all the points belong to invariant tori. Of course if we reduce sufficiently the grid step, at a certain scale we can detect the effect of resonances or chaotic orbits.

The numerical computation of the frequencies $\vec{\nu}$ uses an algorithm proposed by Laskar. Each initial point is iterated N-times by applying the map $\mathcal{M}$ and the projections of the orbit on the coordinate planes (x_j, p_j) are considered. In the case of a regular orbit (i.e. an orbit which belongs to an invariant torus) the projections are a discrete sampling of a quasi-periodic signal and their Fourier transform contains the integer combinations of a finite number of frequencies. By using the Hanning filter and an analytical interpolation of three points around the maximal value of the FFT it is possible to achieve a precision in the position of main frequency which scales according to $1/N^4$ with the iteration number,[14] if the distance between the relevant frequencies is $\gg 1/N$. As a consequence it is possible to get a high precision in the measure of the main frequency with a relative small number of iterations of the map $\mathcal{M}$. If $\mathcal{M}$ is the Poincarè map of the transverse dynamics in a particle accelerator and the nonlinearity are not too strong, the main frequency in each coordinate plane is the betatronic frequency associated with that plane.

The numerical computation of the FM can be extended to the orbits which belong to the resonant regions and to the chaotic regions. In the first case we get the resonant values of the betatronic frequencies and the phase locking phenomenon occurs in the whole resonant region; the grid points in the resonant region are mapped on the resonant line $\vec{k} \cdot \vec{\nu} = n$, where $\vec{k}$ and n are integers. In the second case the result of the FM is very sensitive to the initial condition and the image of the grid points in a chaotic region is a fuzzy cloud of points in the frequencies space. As a consequence the computation of the tune gradient turns out to be a good parameter to distinguish between regular and chaotic orbits and it is possible to introduce a threshold for the gradient, which could be related to the local diffusion velocity in phase space.

The previous properties allow to use the FM to get a global picture of the phase space, where the effect of dominant nonlinear resonances

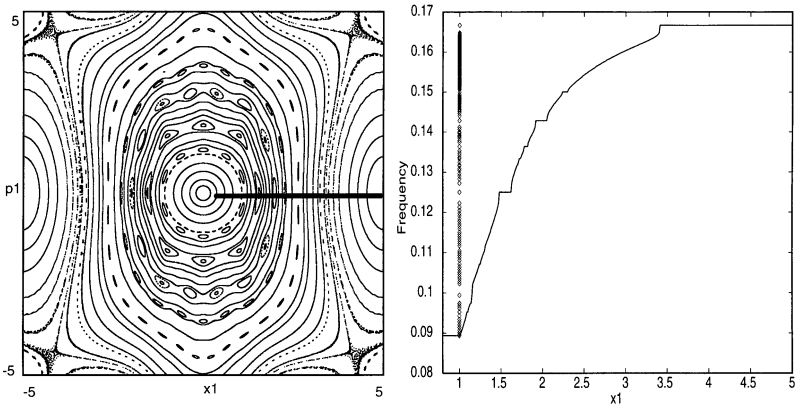

FIGURE 2 Poincarè map and frequency map for a matched beam propagating in our nominal FODO; the initial conditions are restricted to the plane $x_2 = p_2 = 0$ so that we recover a one degree of freedom system and the parameters used in the simulations are ($\xi = 3 \times 10^{-6}$, $K_F = K_D = 12$).

is pointed out and the presence of chaotic regions is detected. Of course the information of the FM becomes more precise, if we increase the number of points in the grid and the number of iterations for each point.

In Figure 2 we illustrate the FM analysis for a one degree of freedom system: we consider the single particle dynamics in our reference FODO channel, taking the section $x_2 = p_2 = 0$; the value of the space charge parameter ξ is enhanced to the value 3×10^{-6} in order to amplify the effect of nonlinear terms. In the left part we show the phase space of the Poincarè map and the stars on the positive x_1-axis are the uniform grid of 500 points where we have computed the FM; the positive x_1-axis is clearly a traverse section of the phase space. In the right part of Figure 2 we plot the horizontal tune ν as a function of the initial condition and the image of the grid is shown by the stars on the vertical axis: from the distribution of the points one can distinguish among the regular orbits, the resonant regions and the chaotic orbits.

Another advantage of the FM is the possibility of an extension to an almost periodically time dependent Hamiltonian systems where a Poincarè section cannot be defined. For example we consider a symplectic map $\mathcal{M}(\vec{\lambda})$ periodically dependent on the parameters $\vec{\lambda}$. The

parameters are changed at each iteration according to $\vec{\lambda} \to \vec{\lambda} + \vec{\alpha}$, where the frequencies $\vec{\alpha}$ do not satisfy any resonant condition. In this case the KAM theory proves the existence of a transformation T from the action angle variables $(\vec{\theta}, \vec{I})$ to the initial variables, which depends on the parameters $\vec{\lambda}$ and such that

$$\mathcal{M} \circ T(\vec{\theta}, \vec{I}; \vec{\lambda}) = T(\vec{\theta} + \vec{\nu}(\vec{I}), \vec{I}; \vec{\lambda} + \vec{\alpha}). \tag{15}$$

All the frequencies $\vec{\nu}, \vec{\alpha}$ do not have to satisfy any resonant condition

$$\vec{k} \cdot \vec{\nu} + \vec{h} \cdot \vec{\alpha} = n \tag{16}$$

where $\vec{k}$ and $\vec{h}$ are integer vectors.

Then we can define the FM by associating with each regular orbit only the frequencies $\vec{\nu}$, which still characterize the orbit. When the frequencies ν_j correspond to the main component of the FFT of the projections of an orbit on the coordinate planes (x_j, p_j), the same algorithm which has been previously described, can be applied. If we choose a uniform grid of points in the transverse section of the phase space, the grid points in the regular regions are smoothly mapped in the frequencies space; the points in the resonant regions are mapped on the resonant lines (16) since the phase locking still occurs; finally the points corresponding to chaotic orbits give a fuzzy cloud of points in the frequencies space.

In the case of the transverse dynamics of a FODO cell when we take into account the space charge effect due to an intense beam lightly mismatched, the Poincarè map turns out to be a two degrees of freedom symplectic map which is modulated by the envelope frequencies α_- and α_+. The domain $\{x_1 \geq 0,\ x_2 \geq 0,\ p_1 = p_2 = 0\}$ is a transverse section of the phase space, if the space charge effect is not too big. The betatronic frequencies of the motion (ν_1, ν_2) correspond to the maximum in the Fourier transform in each coordinates planes and the algorithm of the FM can be applied. This fact is illustrated in Figure 3 where the FFT of the projection of a regular orbit on the (x_1, p_1) plane is shown. We have considered the case #2 of our FODO cell with a 30% mismatched initial condition for the beam envelopes; the highest peak in the FFT corresponds to the horizontal betatronic frequency, whereas the other peaks give all the linear integer combination between the betatronic frequencies and the envelope frequencies.

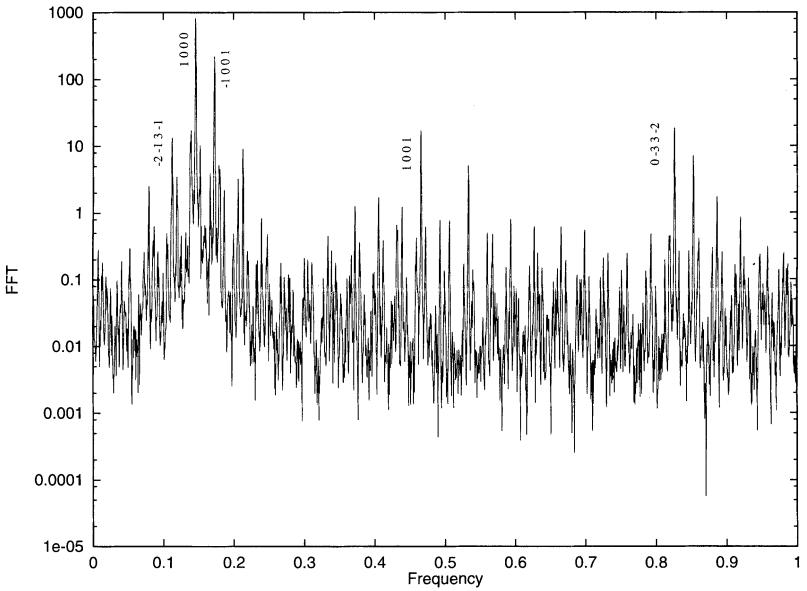

FIGURE 3 FFT of the projection of orbit on the coordinate plane (x_1, p_1) in the case #2 when the beam envelopes are mismatched. The initial condition corresponds to a regular orbit outside the beam core. The peaks are characterized by four integers (k_1, k_2, h_-, h_+) according to the linear combination $\vec{k} \cdot \vec{\nu} + \vec{h} \cdot \vec{\alpha}$ (only a few are indicated in the plot, but 15 resonances are recognized by our code). The strongest resonance (1,0,0,0) is the horizontal tune computed by the FM; the second frequency (0,1,0,0) is determined by the FFT of the projection on the vertical coordinate plane (x_2, p_2).

5 NUMERICAL ANALYSIS

The FM analysis of the two nominal cases has been performed, taking into account matched and mismatched initial conditions. We have computed the FM for a grid of 14 400 points, uniformly distributed in polar coordinates $r = \sqrt{x_1^2 + x_2^2}$, $\phi = \arctan(x_2/x_1)$, in the domain $\{r \leq 5,\ \phi \in [0, \pi/2],\ p_1 = p_2 = 0\}$. The amplitudes x_1 and x_2 are plotted in matched beam envelope units, so that our domain corresponds to 10 times the rms beam envelope. Each orbit corresponds to 1024 iterations of the Poincarè map and the accuracy in the betatronic frequencies given by the FM algorithm has been evaluated by checking the numerical stability of the results when we increase the iterations number. For the regular orbit we have a numerical precision of the order $O(10^{-4})$. Then for each point we have evaluated the tune

gradient according to

$$\Delta\nu = \frac{\|\vec{\nu}(\vec{x} + \delta\vec{x}) - \vec{\nu}(\vec{x})\|}{\|\delta\vec{x}\|} \tag{17}$$

where $\delta\vec{x}$ is a random vector of length 0.0175, which corresponds to half the radial step. The threshold $\Delta\nu_{\text{thr}}$ to distinguish regular and chaotic orbits has been chosen by calculating the maximal value of the gradient (17) in the region of the regular orbits in both the cases. The value $\Delta\nu_{\text{thr}} = 0.03$ is provided by our analysis as it is illustrated in Figure 4; the stability of the regular orbits has also been checked by a tracking program. The relation between the diffusion in the phase space and the different regularity criteria, which can be introduced by the FM analysis or the evaluation of the Ljapounov exponent has been studied in the paper[20] for the circular accelerators. In the linear accelerators, where we are interested to detect the diffusion of few particles in a limited numbers of iterations, the introduction threshold $\Delta\nu_{\text{thr}}$ has the purpose to distinguish the regular regions where no diffusion can be detected from the chaotic regions where there exist orbits which perform large excursions in the phase space. The

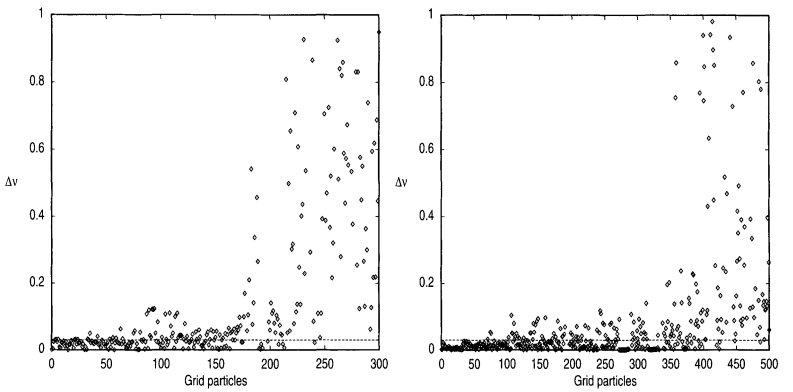

FIGURE 4 Tune gradient computed according to Eq. (17) as a function of the grid points; the points are ordered from left to the right by increasing the polar angle $\phi \in [0, \pi/2]$ and the radial coordinate r; we have plotted the points near the beam core up to the appearance of large fluctuations of the tune gradient which indicates the beginning of a chaotic region. The line corresponds to the chosen threshold for $\Delta\nu$. In the left part we consider the case #1 with 30% of mismatch for the envelope solutions; in the right part we consider the case #2 with the same amount of mismatched.

dynamics of the particles at the boundary of the regular regions can be carefully studied by tracking programs considering a high density of initial conditions in the phase space.

In Figure 5 left we plot the FM for the case #1 for the matched beam. The bottom-left point corresponds to the particles inside the beam core, which suffer the maximum tune depression due to space charge, and the upper-right point corresponds to the particles far from the core, which do not feel any space charge. The intermediate points are the particles that can suffer nonlinear resonances and stochastic behavior. The phase space is dominated by the resonance $\nu_1 = \nu_2$, which creates a channel able to connect the region outside the beam envelope and the region at large amplitude. A chaotic region is visible at large amplitude where both tunes are resonant and several resonant lines cross each other. In Figure 5 right we plot the initial conditions used for the FM, which satisfy the condition $\Delta\nu < \Delta\nu_{\text{thr}}$. As a consequence, the missing points characterize the region where the diffusion could appear according to our criterion. We have a small region of chaotic particles near the beam envelope due to the $\nu_1 = \nu_2$

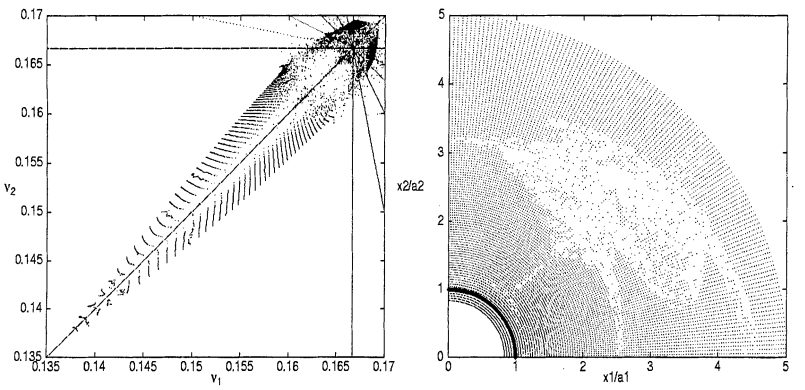

FIGURE 5 Frequency map analysis for the case #1, matched envelope. On the left side the frequencies corresponding to 14400 initial conditions are plotted; the distribution is uniform in polar coordinates, with radius ranging between 0.8 and 5. Some resonance lines can be recognized (high peak density surrounded by vacuum); the resonance lines with $|k_1| + |k_2| \leq 6$ are plotted. On the right side the regular initial conditions ($\Delta\nu > \Delta\nu_{\text{thr}}$) are plotted; the profile of the beam core is drawn in thick black. The axis unities are normalized to the matched beam envelopes $\vec{a}(s)$ and the same convention is used in the other figures.

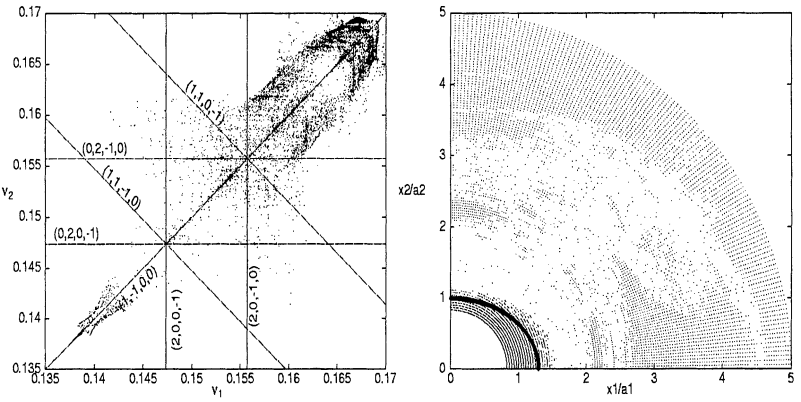

FIGURE 6 FM for the case #1, with 30% beam mismatch ($\delta_1 = 0.3$, $\delta_2 = 0$). On the left side resonance lines with $|k_1| + |k_2| + |h_-| + |h_+| \leq 3$ are plotted. The initial beam envelope is drawn on right side, together with regular points.

resonance, which could become unstable when we consider the mismatched case.

We have then mismatched the envelope initial conditions, by taking $\delta_1 = 0.3$. In this way both the odd and the even envelope modes are excited, since the initial conditions can be decomposed as $(\delta, 0) = \delta(-\vec{\delta}_- + \vec{\delta}_+))/\sqrt{2}$, and new resonances are present in the FM plot (Figure 6) due to the integer combination (16). We have therefore an enlargement of the chaotic region of the $\nu_1 = \nu_2$ resonance because of the overlapping with the new resonances (see Figure 6 left). The bigger chaotic region is clearly visible in Figure 6 right, where we have plotted the stable points according to our criterion and the diffusion is more severe.

We have then chosen a different working point (case #2), so as to avoid the $\nu_1 = \nu_2$ resonance, but at the same time with tunes close enough to satisfy approximately the equipartitioning design criteria, generally adopted for high current linacs.[20,21]

In Figure 7 left and right the FM analysis is shown for the matched beam. The FM still shows several resonant channels, which are well separated and therefore without relevant chaotic regions. The chaotic region due to the $\nu_1 = \nu_2$ is visible in the left part of the picture.

In this case the stable points cover almost all the analyzed region with the exception of very small chaotic areas where only a bounded

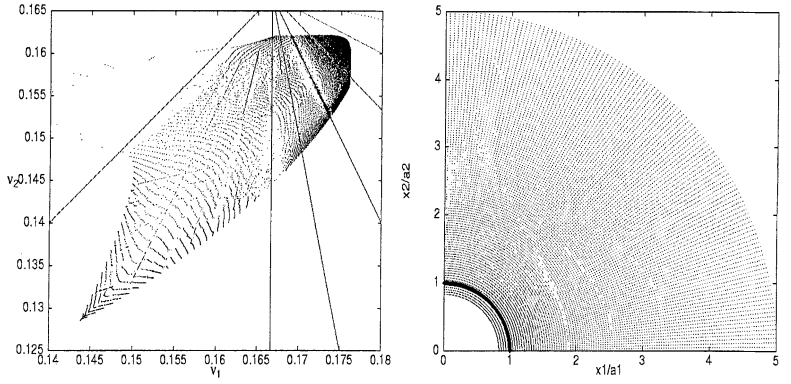

FIGURE 7 FM for the case #2, matched beam; in the left plot resonance lines with $|k_1| + |k_2| \leq 6$ are plotted. In the right plot regular points and beam cross section are shown.

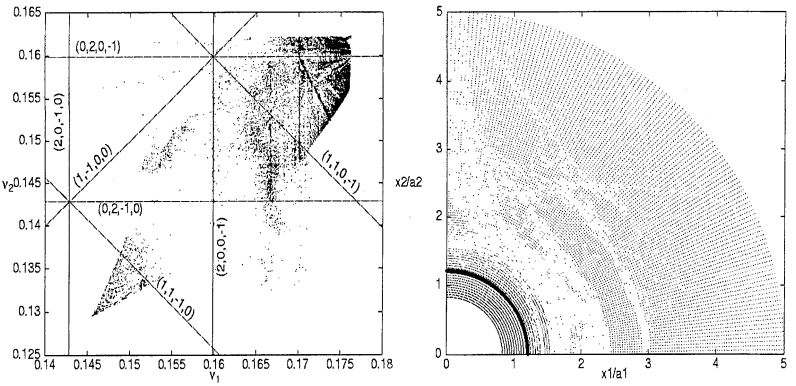

FIGURE 8 FM for the case #2, $\delta_1 = 0.3/\sqrt{2}$, $\delta_2 = 0.3/\sqrt{2}$. On the left side resonance lines with $|k_1| + |k_2| + |h_-| + |h_+| \leq 3$ are plotted. The initial beam envelope is drawn on right side, together with regular points.

diffusion could be detected. When we consider the mismatched case two big resonances appear, creating a large chaotic area in the analyzed region (see Figure 8 left). As a consequence we have chaotic orbits starting from the envelope border (see Figure 8 right), but the maximal amplitude reached by the unstable particles is smaller than the one in case #1.

6 TRACKING RESULTS

We are interested in beam diffusion after 1000 periods, that is a typical number for a long linac.

We therefore choose initial conditions (typically 40 000) in a annulus immediately outside the beam core, between 1 and 1.4 times the beam envelope, and we follow their evolution. The parameter $r_{\max}$, maximum of r during the particle evolution, is used to check the diffusion. In particular in Figures 9–12 for the different cases described in the previous section, we plot the initial conditions used for the tracking, and with a different marker we characterize the particles that have diffused up to an amplitude larger than 2. In each case this plot is compared with the plot related to the $\Delta\nu$ criterion with the same scale. The comparison confirms our criteria; indeed for the matched case #1 the $x=y$ channel is very small, and there is no diffusion. Whereas, when a 30% mismatch is added, a large region with $\Delta\nu > \Delta\nu_{\text{thr}}$ appears (Figure 10 right), and correspondingly many particles diffuse (Figure 10 left).

For the case #2 matched the FM analysis gives only regular points and indeed the tracking does not show any diffusion. Adding therefore 30% mismatch we can see a diffusive region, foreseen by the FM analysis.

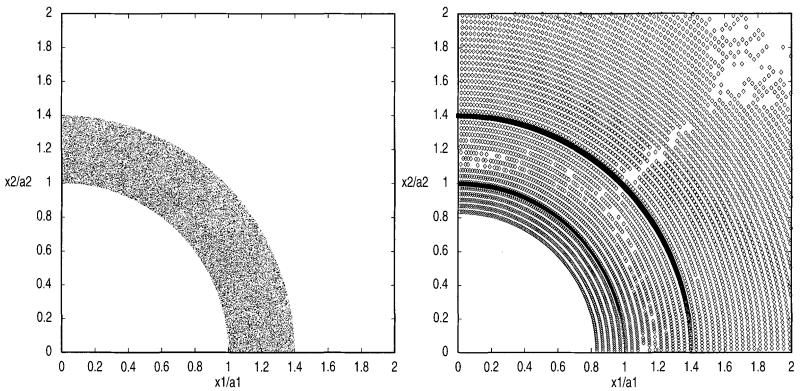

FIGURE 9 Results of tracking for case #1, matched. In the left part 10 000 initial conditions chosen for tracking are shown; different markers are used for the points that diffuse up to $r_{\max} \geq 2$ (no one in this case). In the right plot for comparison the result of the FM analysis on the same scale is shown; The annulus used for tracking initial conditions is also drawn.

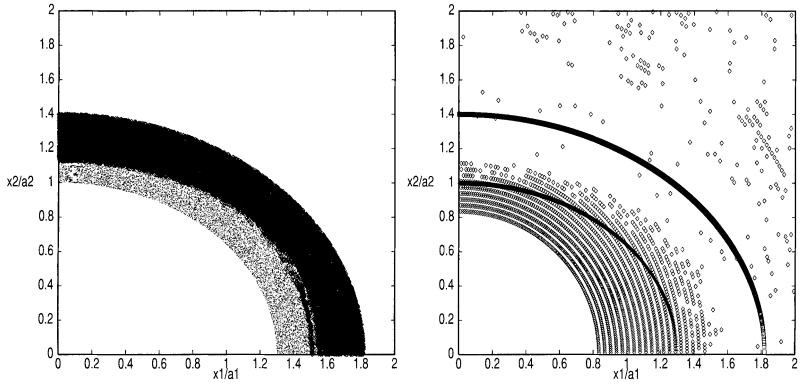

FIGURE 10 Results of tracking for case #1, 30% mismatch ($\delta_1 = 0.3$, $\delta_2 = 0$). In the left part 10 000 initial conditions chosen for tracking are shown; different markers are used for the points that diffuse up to $r_{\max} \geq 2$. In the right plot for comparison the result of the FM analysis on the same scale is shown.

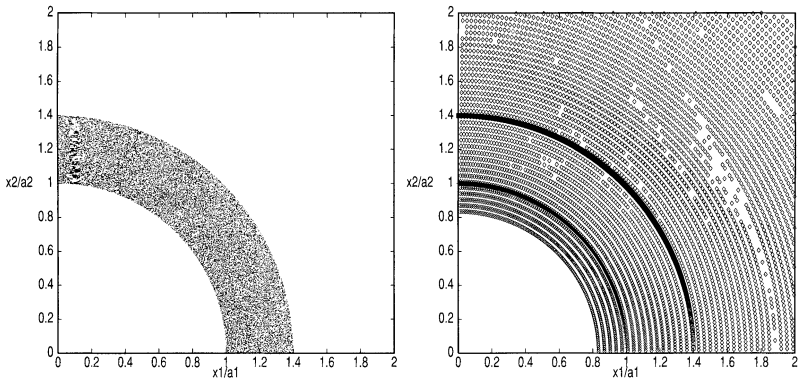

FIGURE 11 Results of tracking for case #2, matched. In the left part 10 000 initial conditions chosen for tracking are shown; different markers are used for the points that diffuse up to $r_{\max} \geq 2$ (no one in this case). In the right plot for comparison the result of the FM analysis on the same scale is shown.

We can therefore conclude that we did not see any diffusion in the points that are regular according to FM $\Delta\nu$ criterion. This result gives a powerful means to optimize the tracking.

As an example, we have done a systematic study of the diffusion as a function of the beam mismatch in both cases. The possibility to concentrate the test particles in the dangerous regions gives an

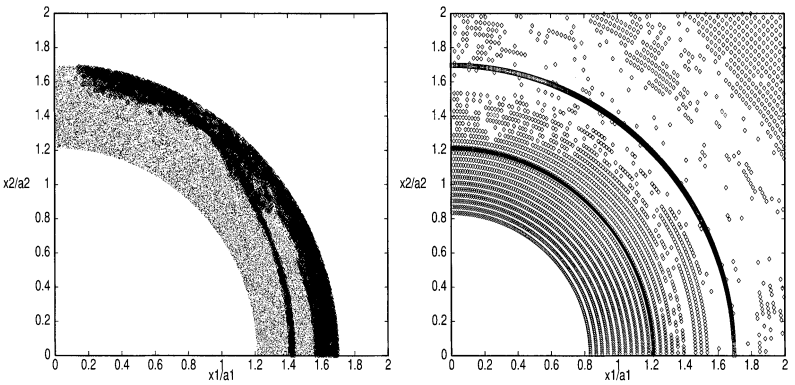

FIGURE 12 Results of tracking for case #2, mismatched ($\delta_1 = \delta_2 = 0.3/\sqrt{2}$). In the left part 10 000 initial conditions chosen for tracking are shown; different markers are used for the points that diffuse up to $r_{\max} \geq 2$. In the right plot for comparison the result of the FM analysis on the same scale is shown.

enhancement of the sensitivity of these runs, with a reasonable CPU time. It should be noted that the test particles have been chosen, for every mismatch, in a region that includes the chaotic region for the maximum beam mismatch considered. This results in a safety margin for the cases with lower mismatch.

In Figures 13 and 14 $R_{\max}$ as a function of the mismatch $\|\vec{\delta}\|$ is shown; in this case $R_{\max}$ is the maximum $r_{\max}$ (maximum r during the 1000 periods tracking) among all the particles of the sample. The initial conditions correspond to the region between 1 and 1.2 times the beam envelope. For the case #1 the simulations have been done for three different kinds of mismatch, $\delta_1 = -\delta_2$, $\delta_1 = \delta_2$ and $\delta_2 = 0$, corresponding to $\delta\vec{\delta}_-$, $\delta\vec{\delta}_+$ and $\delta(-\vec{\delta}_- + \vec{\delta}_+)/\sqrt{2}$. The first condition excites the envelope odd mode, the second the even mode, the third both modes. For each mismatch condition we performed 10 runs with 10 000 particles; due to our model each run is clearly independent, so that the largest of the ten $R_{\max}$ corresponds for each mismatch case to the maximum displacement calculated with 100 000 particles, while the spread gives an idea of the statistical properties of the diffusion estimate.

In the symmetrical case one can see that the excitation of the odd mode is more dangerous than the excitation of the even mode.

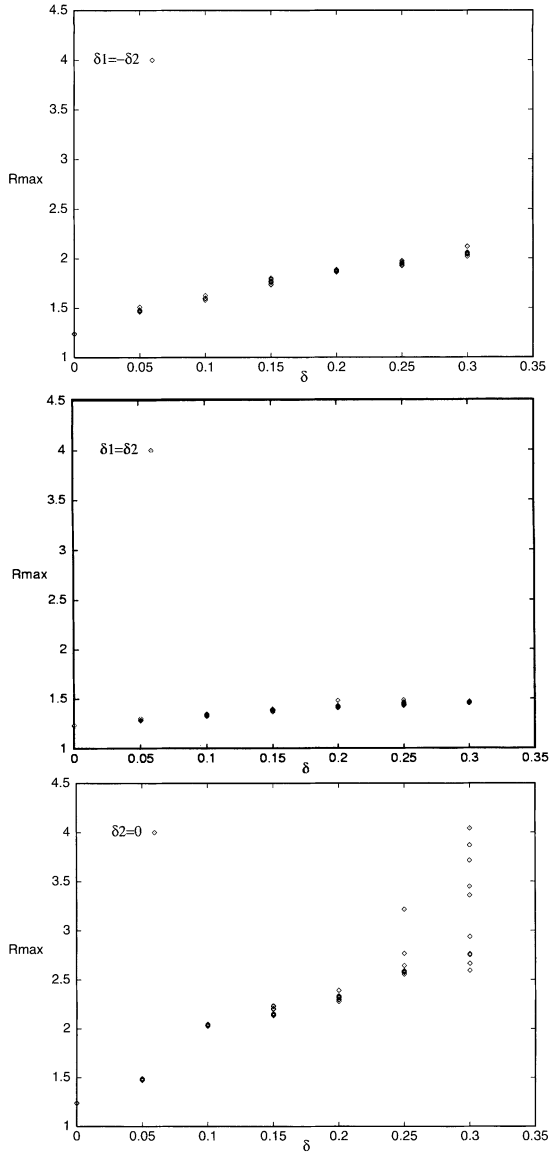

FIGURE 13 Results of the systematic tracking for case #1. Each point gives $R_{\max}$ (maximum particle displacement in a 1000 period running among a sample of 10000 test particles) as a function of δ (norm of the displacement vector). For each value of δ ten different samples are plotted, so to have the maximum and the spread. Moreover in the three graphs we have three different sets of simulations with initial mismatch, in the order, $\delta_1 = -\delta_2$, $\delta_1 = \delta_2$ and $\delta_2 = 0$, corresponding to $\delta\vec{\delta}_-$, $\delta\vec{\delta}_+$ and $\delta(-\vec{\delta}_- + \vec{\delta}_+)/\sqrt{2}$.

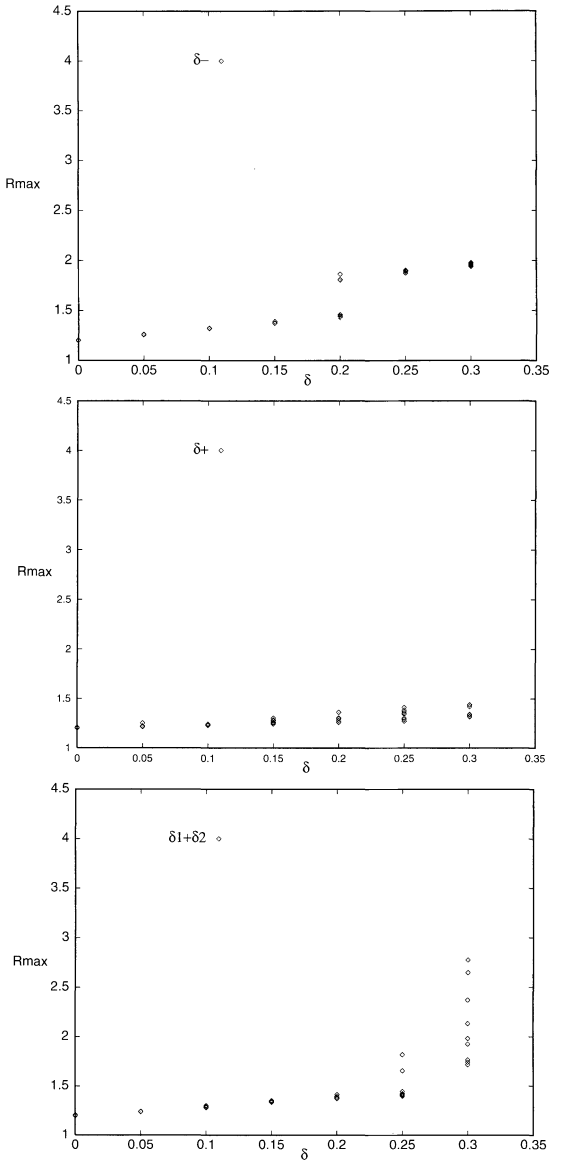

FIGURE 14 Results of the systematic tracking for case #2. Each point gives $R_{\max}$ (maximum particle displacement in a 1000 period running among a sample of 10 000 test particles) as a function of δ (norm of the displacement vector). For each value of δ ten different samples are plotted, so to have the maximum and the spread. Moreover in the graph we have three different sets of simulations with initial mismatch corresponding, in the order, to $\delta\vec{\delta}_-$, $\delta\vec{\delta}_+$ and $(\delta, \delta)/\sqrt{2} = (0.49\vec{\delta}_- + 0.86\vec{\delta}_+)/\sqrt{2}$.

Moreover we remark that when both modes are excited, so that we can have resonances due to the linear combinations of all four main frequencies, the maximum displacements are the largest.

For the case #2 we have done the simulations for initial conditions corresponding to $\delta\vec{\delta}_-$, $\delta\vec{\delta}_+$ and $(\delta,\delta)/\sqrt{2}$(Figure 14). The first two conditions give normal modes, in the third case we have a significant mode mixing ($\vec{\delta} = 0.49\vec{\delta}_- + 0.86\vec{\delta}_+$). We observe that the mode mixing leads to a condition where resonances, involving four frequencies, can be excited, and as a consequence it represents the worst condition for beam stability and diffusion is enhanced. However we observe that the case #2, which avoids the $\nu_1 = \nu_2$ resonance, is anyway better than case #1.

As a final point we have some remarks about the FODO model. The representation described in Section 2, which has the advantage of being self-consistent and largely studied in previous literature, is characterized by a very localized zone of nonlinearity, immediately outside the beam core. In other words we follow a diffusion (from envelope surface to large amplitude) driven by a nonlinear force that vanishes as $1/r$. As a consequence at large amplitude the motion is again regular and bounded; the maximum amplitudes found in this paper are of about 4 times the beam envelope, i.e. 8 times the beam rms size. These values would probably increase in a more realistic model, when one considers other nonlinearities, like multipole errors in the quadrupoles and Bessel function dependencies of the transverse RF field, that have a polynomial dependence on transverse coordinates; nevertheless the same analysis can be applied.

The small differences among the FODO cells typical of a single pass focusing channel, could be treated as stochastic perturbations of an average beam dynamics and the results of the FM analysis would be useful to get a better understanding of the tracking results in presence of machine errors.

The approach shown in this paper could be extended without major changes to the 3D problem of a bunched beam propagating in a periodic system (introducing for example the RF cavities with synchronous phases $-90°$). The study of a linear accelerator, that is not exactly a periodic system, requires a some where different investigation, with the choice of appropriate adiabatic invariant variables.

7 CONCLUSIONS

The FM turns out to be an efficient tool to represent the phase space of multidimensional hamiltonian systems. It allows to detect the position of the resonances and the chaotic regions with a high accuracy and it can be used for quasi-periodic time dependent systems with two or more degrees of freedoms when the direct plot of the phase space is not possible.

Our analysis of the transverse dynamics of an intense beam in a FODO cell shows very well the role of the beam mismatching in exciting the various resonances related with the beam modes. The importance of the initial mismatched beam configuration, in addition to the mismatch amplitude, is pointed out. The consequent appearance of diffusive zones has been analyzed, and a criterion for the determination of stable regions has been introduced. This criterion has been checked with the help of tracking.

References

[1] M. Prome, *Proceedings of 1996 International Linac Conference*, Geneva, CERN 96–07, p. 9 (1996).
[2] J.-M. Lagniel, *Proceedings EPAC 96 Conference*, Sitges 1996, Institute of Physics Publishing, Bristol and Philadelphia, (1996) p. 210.
[3] R.L. Gluckstern, *Proceedings of the 1994 international Linac Conference*, Tsukuba, (1994) p. 333.
[4] J.-M. Lagniel *Nucl. Instr. Meth.*, **A 345**, 405–410 (1994).
[5] Qian Qian, R.C. Davidson and C. Chen, *Phys. Plasmas*, **2**(7), (July 1995) p. 2674.
[6] M. Reiser and T. Wangler, *Proceedings of 1991 PAC conference*, IEEE 91CH3038-7 (1991) p. 251.
[7] I. Kapchinsky and V. Vladimirsky in *Proceedings of the International Conference on High Energy Accelerators and Instrumentation*, CERN 1959, p. 274.
[8] J. Laskar, *Icarus*, **88**, 266, (1990).
[9] J. Laskar, *Physica D*, **67**, 257 (1993).
[10] A. Pisent *et al.* "Frequency Map Analysis of the Chaotic motion of an intense mismatched beam in a FODO channel" to be published as a DESY internal report (1997).
[11] H.S. Dumas and J. Laskar, *Phys. Rev. Lett.*, **70**, 2975 (1993).
[12] J. Laskar and D. Robin, *Particle Accelerators*, **54**, 183 (1996).
[13] R. Bartolini, A. Bazzani, M. Giovannozzi, W. Scandale and E. Todesco, *Particle Accelerators*, **52**, 147, (1996).
[14] R. Bartolini, A. Bazzani, M. Giovannozzi, W. Scandale and E. Todesco, *Particle Accelerators*, **55**, 247 (1996).
[15] F.J. Sacharer, *IEEE Trans. Nucl. Sci.*, **NS-18**, 1105 (1971).
[16] P. Lapostolle, *IEEE Trans. Nucl. Sci.*, **NS-18**, 1101 (1971).
[17] J. Struckmeier and N. Reiser, *Part. Acc.*, **14**, 227–260 (1984).
[18] V.I. Arnold, *Russ. Math. Surv.*, **18**(6), 85 (1963).

[19] J. Poeshel, *Commun. Pure Appl. Math.*, **35**(1), 653 (1982).
[20] M. Giovannozzi, W. Scandale and E. Todesco *Part. Accel.*, **56** 195–225 (1997).
[21] M. Reiser, *Theory and design of Charged Particle Beams* John Wiley and Sons, Inc. New York, NY 1994, pp. 573–580.
[22] S. Nath *et al. Front End Physics Design of the APT Linac* Geneva, CERN 96-07, p. 680 (1996).